Soft Matter

PAPER

View Article Online
View Journal | View Issue

Cite this: *Soft Matter*, 2021, **17**, 1368

The role of entropy in wetting of polymer brushes†

Liz I. S. Mensink,[a] Sissi de Beer *[b] and Jacco H. Snoeijer [a]

The wetting of polymer brushes exhibits a much richer phenomenology than wetting of normal solid substrates. These brushes allow for three wetting states, which are partial wetting, complete wetting and mixing. Here, we study the transitions between these wetting states for brushes in contact with polymer melts and compare them to predictions using enthalpic arguments based on brush and melt interactions. We show that the transitions are shifted compared to the enthalpic predictions and that the shifts can be positive or negative depending on the length of the melt polymer and the brush grafting density. The reason for this is that these brush and melt parameters can have a positive or negative effect on the entropic contribution to the free energy of the system. Our results highlight the relevance of entropy in predicting the exact wetting transitions, which is important for the design of brush-based coating applications.

Received 27th January 2020,
Accepted 29th November 2020

DOI: 10.1039/d0sm00156b

rsc.li/soft-matter-journal

1 Introduction

Polymer brushes consist of long macromolecules densely end-attached to a surface.[1] They are popular building blocks in the design of functional surface coatings due to their versatility and simplicity to manipulate.[2,3] For example, these brushes have been employed as smart sensors[4–6] or to manage surface lubricity[7–9] and adherence.[10,11] Surface wettability is also tuned straightforwardly with polymer brushes, which has resulted in the development of moisture management systems[12] and self-cleaning surfaces.[13] For these applications, it is important to understand the wetting of polymer brushes.

Wetting of polymer brushes deviates from wetting behavior on solid surfaces.[14,15,60] Solids can be either partially or completely wetted. In contrast, polymer brush coatings can also absorb liquids, which gives rise to three wetting states, partial and complete wetting and the mixed state.[16,17] The wetting state of the system depends on the brush–liquid interactions and the self-affinity of the brush (see Fig. 1). The three different states are separated by two transition-lines: the mixing to demixing transition (dashed) and the complete to partial wetting transition (dash-dot). To a large extent, these transitions can be understood using enthalpic arguments. When the affinity of the brush with the liquid, ε_{BL}, is less strong than the average self-affinities for the brush, ε_{BB}, and the liquid, ε_{LL}, the transition from mixing to demixing will occur. This happens when one goes from left to right crossing the vertical gray dashed line, $W = \varepsilon_{BB} + \varepsilon_{LL} - 2\varepsilon_{BL} = 0$, in Fig. 1. If the self-affinity of the liquid, ε_{LL}, is stronger than the affinity of the brush with the liquid, ε_{BL}, a transition from complete wetting to partial wetting can be observed. This happens

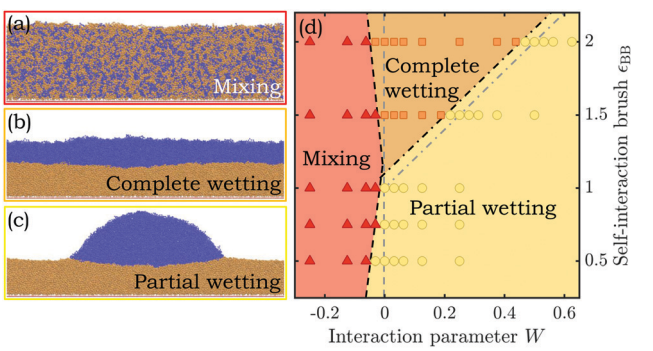

Fig. 1 (a–c) Snapshots of simulation cells showing a polymer droplet (blue), interacting with a polymer brush (orange) for the three wetting states. (d) Interaction-based phase diagram depicting the relation between the states of wetting and brush self-interaction ε_{BB} and the interaction parameter W. Observed are mixing (red triangles), complete wetting (orange squares) and partial wetting states (yellow circles). The gray lines indicate the enthalpic predictions for the mixing to demixing transition ($W = \varepsilon_{BB} + \varepsilon_{LL} - 2\varepsilon_{BL} = 0$, dashed) and the transition from complete to partial wetting ($\varepsilon_{BL} = \varepsilon_{LL}$, dash-dot). The black lines give the transitions observed in the MD simulations of ref. 17.

[a] *Physics of Fluids and the MESA+ Institute, University of Twente, PO box 217, 7500 AE Enschede, The Netherlands*
[b] *Sustainable Polymer Chemistry and the MESA+ Institute, University of Twente, PO box 217, 7500 AE Enschede, The Netherlands. E-mail: s.j.a.debeer@utwente.nl; Tel: +31 53 4893170*

† Electronic supplementary information (ESI) available: (1) Snapshots and density profiles for increasing N displaying the transition from mixing to complete to partial wetting, (2) brush swelling as a function of the self-interaction between the polymers and (3) surface tension calculations for the melt. See DOI: 10.1039/d0sm00156b

when one goes from left to right, crossing the inclined gray dash-dotted line in Fig. 1. Though these enthalpic arguments capture the global behavior, there are clear deviations between the predicted transitions (gray) and the transitions extracted from recent molecular dynamics (MD) simulations[17] (black). These deviations have been attributed to entropic effects.[17] Yet, to what extend and in what direction entropy can affect these deviations is not yet studied in detail.

In this paper, we will elucidate the role of entropy in the prediction of the wetting phase diagram of brushes wetted by polymeric nanodroplets. From early work on the wetting of brushes by chemically identical polymer melts, it is known that entropic effects can cause counter-intuitive phenomena such as demixing[14,16,18–23] between the brush and the melt. This effect has been observed to strongly depend on the grafting density and the molecular weight of the melt and can result in autophobic dewetting,[14,16,22,24,25] where melt droplets are formed on the chemically identical brush.

To understand the phenomena of demixing of chemically identical brushes and melts, reported previously,[14,16,18–23] one needs to consider the different entropic contributions to the free energy.[18] Without end-grafting of brush-polymers, melt and brush-polymers would mix to gain translational entropy. However, since brush-polymers are constrained, they cannot gain translational entropy upon mixing. Instead, their entropy is reduced by mixing due to the elastic penalty for stretching upon absorption of the melt. Because brush stretching depends on the grafting density of the brush, the mixing to demixing transition depends on the grafting density as well.[18,19,26] Moreover, the translational entropy depends on the length of the melt-chains and, therefore, the mixing to demixing transition depends on the polymer length too.[18,19,26]

To understand autophobic dewetting, as reported previously,[14,22,24,25] we have to consider the effect of entropy on the spreading parameter S. The spreading parameter is defined as $S = \gamma_{BV} - (\gamma_{BL} + \gamma_{LV})$, where γ_{BV}, γ_{BL} and γ_{LV} are the interfacial tensions between the solid brush and vapor phase (BV), the brush and liquid melt phase (BL) and the melt and vapor phase (LV), respectively. When the spreading parameter is positive ($S > 0$), complete wetting occurs and the droplet will partially wet the surface when $S < 0$. The interfacial tension between chemically identical brushes and melts γ_{BL} is negatively proportional to the difference in entropy before and after bringing the brush and melt in contact. For short melt polymers and low grafting densities, the change in entropy is positive. Contrarily, the change in entropy is negative for long melt polymers and high grafting densities. Thus, complete wetting is observed for short chains and low grafting densities, while partial wetting is observed for large chains and high grafting densities.[14,22,24,25]

The above described demixing and autophobicity effects are well characterized for brush–melt systems that are chemically identical.[18–23] Yet, for many applications, the brushes will be in contact with chemically distinct media.[27–29] The role of entropy in wetting and, in particular, the wetting transitions for brush–melt systems of chemically distinct media is still largely unexplored and we address this in the present paper, where we study the role of entropy on the wetting transitions of polymer brushes wetted by polymer droplets, using MD simulations.

2 Model and methods

We use a coarse-grained polymer model, based on the bead-spring model initially developed by Kremer and Grest.[30] This model is well-known to qualitatively reproduce the static and dynamic response of polymer brushes.[31–33] Non-bonded interactions within this model are described using the Lennard-Jones (LJ) potential:

$$V_{LJ} = 4\varepsilon\left(\left(\frac{\sigma}{r}\right)^{12} - \left(\frac{\sigma}{r}\right)^{6}\right) \quad (r < r_c), \tag{1}$$

using $\sigma = 1$ and a cut off length $r_c = 2.5\sigma$. The potential is shifted by its potential-value at the cut-off length.

Throughout this paper, we will employ Lennard-Jones units in which σ and ε define the units of length and the unit of energy, respectively. Considering for example poly(ethylene), these units can be converted to real values for the polymers using $\varepsilon = 30$ meV and $\sigma = 0.5$ nm.[34] We use a finite extensible nonlinear elastic (FENE) potential combined with the repulsive part of the Lennard-Jones potential to describe the bonded interactions between consecutive beads within the polymer chains:

$$V_{KG} = -0.5kR_0^2 \ln\left[1 - \left(\frac{r}{R_0}\right)^2\right] + 4\varepsilon\left[\left(\frac{\sigma}{r}\right)^{12} - \left(\frac{\sigma}{r}\right)^{6}\right] + \varepsilon. \tag{2}$$

For V_{KG}, the LJ interaction parameters are $\varepsilon = 1$, $\sigma = 1$ and $r_c = 2^{1/6}\sigma$ and we use a stiffness of $k = 30\varepsilon/\sigma^2$ and a maximum extension $R_0 = 1.5\sigma$, which ensures that there is no bond-crossing.[30] Considering poly(ethylene), the unit of mass [m] is 10^{-22} kg and the unit of time [τ] represents 0.3 ns.[34]

Fig. 2(a) shows a typical snapshot of our simulation cell. The snapshots are rendered using VMD.[35] Our simulation cells consist of a wall composed of single layer of Lennard-Jones particles (red) in a triangular lattice with polymers (orange) anchored by one end to the wall particles. Each individual brush-polymer consists of $N_B = 100$ repeat units for all simulations presented. The density at which these polymers are attached to the surface is varied as $\sigma_{GD} = 0.067, 0.15, 0.2, 0.27$

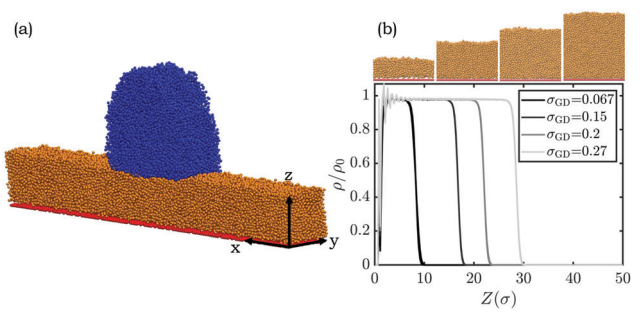

Fig. 2 (a) A typical snapshot of a quasi-2D simulation set-up of a polymer droplet (blue) partially wetting a polymer brush (orange). (b) A graph showing the polymer brush density profile for polymer chains grafted at different grafting densities (σ_{GD} = 0.067, 0.15, 0.2, 0.27 chains per σ^2). Snapshots show corresponding brushes.

chains per σ^2, which equals approximately 1.3, 3, 4 and 5.3 times the critical grafting density for brush formation under poor solvent conditions. For grafting densities above this critical grafting density, the system is in the brush regime. For grafting densities below the critical grafting density, the system is in the so-called mushroom regime. This means our simulations are performed in the brush regime, which is also apparent from the snapshots and density profiles given in Fig. 2(b). They show a step-wise change in the brush density, which is clearly different from the strong variation in density observed for the mushrooms that are formed at densities below the critical grafting density.[36]

The polymer brush is in contact with a uniform polymer melt with a constant chain length that is varied between $N = 2$ and $N = 64$ for individual simulations. The total number of beads present in the polymer melt is kept constant, so the amount of molecules wetting the brush is varied (for $N = 2$ there are 8000 melt molecules, for $N = 64$ we simulated 250 melt molecules).

Our simulations are performed at a constant box-size and volume V, in a quasi-2D setup, as shown in Fig. 2(a). Our simulation box is periodic in x and y, with a boxlength in x of at least 108σ, depending on the spreading of the droplet. For small contact angles, we increased the boxsize in x to 218σ. The boxlength in y is limited to 15σ to suppress Rayleigh instabilities in the infinitely long cylindrical droplet. Yet, it is large enough to ensure that there are no self-interactions between polymer chains (gyration radius for the largest polymers of $N = 64$ is smaller than 6σ). Moreover, in this setup line-tension effects are negligible for droplets with radii that are larger than $R_d = 7\sigma$.[37] Our droplets are all larger than $R_d = 21.5\sigma$. For such large radii, the difference between 3D and 2D contact angles are less 2 degrees.

The equations of motion are solved using the velocity Verlet algorithm as implemented in LAMMPS,[38] using a timestep of $\Delta t = 0.005\tau$. The simulations are performed in the NVT ensemble. The temperature T is kept constant at $k_BT = 1\varepsilon$ (k_B being the Boltzmann constant) using a Langevin thermostat with a damping coefficient of $\xi = 1\tau^{-1}$. The simulation cells are equilibrated for 10^7 timesteps before the production runs of 10^7 timesteps during which the observables are extracted.

From the production runs we extract the density of the brush and the melt as a function of the distance from the wall in slabs of 0.2σ. From these density profiles overlap integrals are calculated, which equal the product of the brush and the melt density integrated over the distance:[39] $N_{ov} = \int_0^\infty \rho_M(z)\rho_B(z)dz$, with ρ_M and ρ_B representing the densities of melt and brush, respectively. These overlap integrals are employed to determine whether the brush and the melt have mixed or not. For the mixed state, the overlap integral will reach a maximum value. From this maximum overlap value, we determine the mixing to demixing transition to occur at 50% of this maximum. We note that the transition between the mixed state is not sharp, but instead evolves gradually *via* partial penetration starting at the top of the brush,[17,21,40,41] as visualized in the ESI,† Fig. S1. We also compute the contact angle of the melt droplet from the production runs, by fitting spherical caps to the isodensity contours of the droplet, following a procedure previously reported.[37]

To tune the affinity between the brush and the melt, relative to the self-interaction of the brush, we alter the strength of the Lennard-Jones potential *via* ε. We study two different strengths for the self-interaction of the brush ε_{BB}, namely $\varepsilon_{BB} = 1$ and $\varepsilon_{BB} = 1.5$. When ε_{BB} is high enough, polymer brushes are attracted to one another, resulting in a collapsed polymer brush structure. We checked that for these ε_{BB}'s, the bare brushes are indeed in the collapsed state (see ESI,† Fig. S2). This is in contrast to simulations by others *et al.*,[42] where brush-wetting was studied for low ε_{BB} and, thus, (implicit) good solvent conditions. Similarly to soft elastomers,[43–47] brushes can deform due to surface tension and form wetting ridges.[48] Due to our choice of ε_{BB}, the brushes are relatively hard and wetting ridges are small and do not affect the macroscopic contact angle.[17]

We vary the interaction between the polymer brush and polymer melt ε_{BL} between 0.375 and 1.5, while $\varepsilon_{LL} = 1$ is kept constant, so that we move through the interaction-based phase diagram from Fig. 1(d) along horizontal lines. From the simulations, we aim to extract generic relations and we do not intend to model particular types of polymers. We allow all sorts of interactions, including interactions of entropic origin, and do not limit this to van der Waals potentials. Therefore, mixing rules do not apply[49] and we can vary ε_{BB} and ε_{BL} independently from each other. The interactions between the wall and the polymer- and liquid-beads is kept purely repulsive ($\varepsilon = 1$, $\sigma = 1$ and $r_c = 2^{1/6}\sigma$) to prevent preferential adsorption near the wall[50] and higher order wetting transitions.[51]

3 Results and discussion

3.1 Mixing–demixing

First, we discuss the results of the MD simulations, addressing the mixing to demixing transition. In our simulations, we varied the grafting density and melt polymerization, for varying values of $W = \varepsilon_{BB} + \varepsilon_{LL} - 2\varepsilon_{BL}$ and for two values of ε_{BB}. Generally, the calculation of relative excluded volumes instead of ε's is preferred to determine mixing–demixing transitions.[52,53] However, conclusions will only be qualitatively different when liquid and polymer particles are not the same size.[54] In our systems all particles have the same size such that qualitative differences due to this simplification are expected to be minor.

From the simulations, we first determine whether the system is in a mixed or demixed state. This was done using the overlap integral of density profiles for the brush and the polymer melt. A high overlap integral means that mixing occurs, whereas a low overlap integral indicates demixing. By taking the overlap integral for several values of W, data-sets were gathered for constant values of N and σ_{GD}. These data-sets were then interpolated to determine whether each data point was above or below the transition-point. The resulting six phase diagrams are given in Fig. 3, where the red squares denote a mixed state and the orange

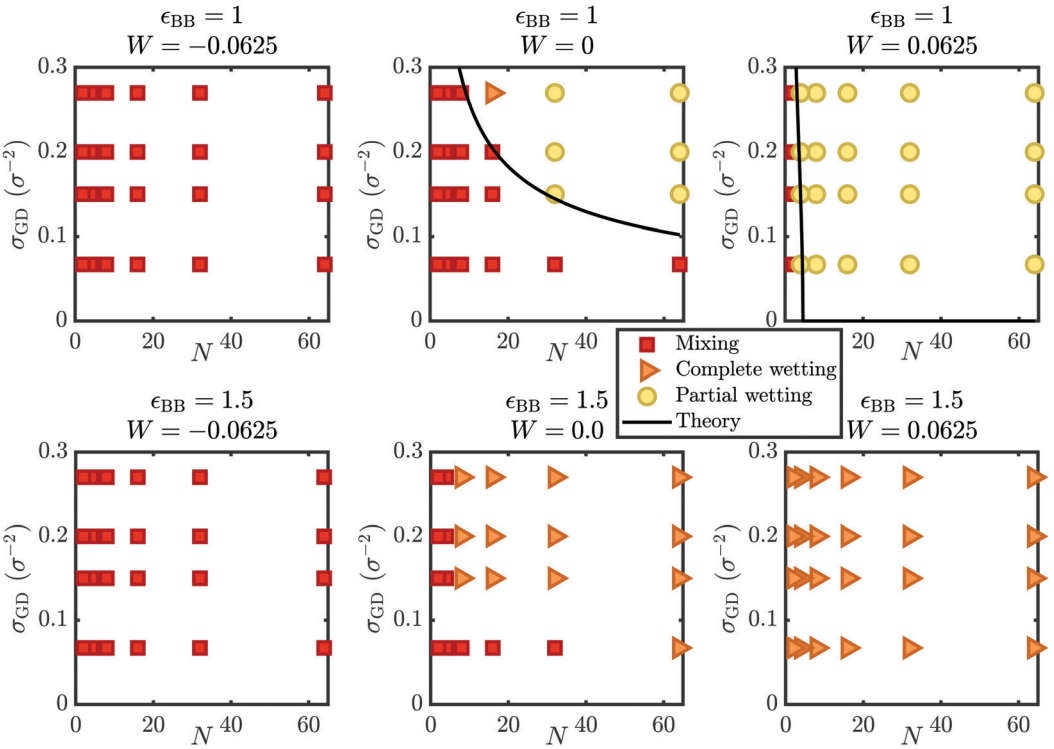

Fig. 3 Geometry-based phase diagrams showing the influence of the grafting density (σ_{GD}) *versus* the degree of polymerization of the melt (N), on the wetting behavior of the brush-melt system. The top row gives simulation-results for brush interactions ε_{BB} of 1.0, the bottom row is at ε_{BB} = 1.5. The left column shows the phase diagram for an interaction parameter W of −0.0625, the middle for 0.0, and the right column at 0.0625.

triangles or yellow circles represent the demixed (complete or partial) wetting state. We call these phase diagrams, geometry based phase diagrams, in contrast to the interaction based phase diagram of Fig. 1.

The different phase diagrams in Fig. 3 from left to right display the results for varying values for the interaction parameter W, and from top to bottom the brush–brush interaction strength ε_{BB}. These geometry-based phase diagrams illustrate that there is a shift in the mixing to demixing transition for chemically distinct melts wetting a brush, compared to the chemically identical wetting case at W = 0. The top row shows the mixing transition for ε_{BB} = 1.0 and the bottom row shows ε_{BB} = 1.5. In the left and right columns, we show the effect of a shift in the interaction parameter to an increased and a decreased net attraction (ΔW = ±0.0625). From the top row (ε_{BB} = 1.0), we see that for W = −0.0625 (top left), only mixing occurs for our settings. These results are in qualitative agreement with previous observations for brush-coated particles in a polymer matrix.[55] Only for very high grafting densities and melt chain lengths, which are not studied in the present work, one would expect to see a transition for such a negative interaction parameter.

For W = 0 (top middle in Fig. 3), we see a mixing to demixing transition. For high grafting densities and long melt-polymers, the system is in the demixed state. For these geometric conditions, there is an entropic penalty for mixing, because long melt polymers cannot gain much translational entropy by mixing and the entropic penalty for stretching is high for the already stretched polymers in high density brushes. In contrast, short polymers can gain much more translational entropy by mixing and the polymers in low density brushes stretch only little upon mixing, such that there is an effective entropy gain when short polymers are absorbed by low density brushes. Thus, mixing will occur for these geometric conditions.

For W = 0.0625 (top right in Fig. 3), the mixing to demixing transition has shifted to lower N and σ_{GD}. Under these conditions, the gain in translational entropy upon mixing needs to overcome the entropic costs of stretching brush polymers and the attractive interactions within the brush and the melt. Therefore, there is mixing for very short polymers (N = 2) only.

In the bottom row (ε_{BB} = 1.5), we observe no phase transitions for W = −0.0625 (bottom left), where we observe only mixing, and for W = 0.0625 (bottom right), where we instead observe only demixing. For W = 0, (bottom middle) we observe a phase-transition similar to the one for W = 0 and ε_{BB} = 1.0, but shifted downward, implying that demixing occurs for shorter chains compared to ε_{BB} = 1.0. From this we can conclude that the free energy cost to stretch the brush polymers has increased, which is consistent with the stronger interaction between the brush polymers.

To predict the transition between mixing and demixing, we will briefly discuss the theoretical work of ref. 19, which has been based on ref. 56. For chemically identical melts and droplets, the free energy in a mean field approximation is given by:

$$\frac{F}{k_B T} = \frac{L^2}{a^2 N_B} + \frac{a^3}{N}\frac{N_B^2}{LD^2}. \quad (3)$$

where L is the height of the brush, N is the chain length of the melt polymers, N_B is the chain length of the brush polymers, a is the effective monomer size and D is the distance between the anchorpoints given by $D = a\sigma_{GD}^{-1/2}$. The first term of eqn (3) represent the entropic penalty that the polymers in the brush pay upon stretching. The second term arises due to excluded volume interactions between the polymer- and/or melt-beads in the system. Using eqn (3), a geometry-based phase diagram can be constructed,[18,19,26,56] showing the effect of varying grafting densities and degrees of melt polymerization. The boundary between the mixed and the demixed state can be found by minimizing eqn (3) with respect to the height of the brush L, resulting in:

$$L \propto aN_B N^{-1/3}\sigma_{GD}^{1/3}. \quad (4)$$

As expected, higher grafting densities result in higher, more stretched polymer brushes. Moreover, upon increasing N, the brush height decreases. When employing that the brush-density of a dry brush is of order one and given by $\rho = N_B\sigma_{GD}a^3/L$, we can substitute eqn (4) to obtain the boundary between dry unmixed and mixed brushes to be:

$$\sigma_{GD,tr} \propto N^{-\frac{1}{2}}, \quad (5)$$

where $\sigma_{GD,tr}$ is the transition grafting density above which the melt and the brush demix.

Eqn (3) can be modified to also take into account cases where the brush and melt are chemically distinct.[19,56] In such cases, enthalpic interactions are incorporated using the Flory–Huggins interaction parameter $\chi = \frac{z}{2k_BT}(\varepsilon_{BB} + \varepsilon_{LL} - 2\varepsilon_{BL})$, with z being the coordination number, which is related to average number of neighbors of a polymer unit. The Flory Huggins parameter is proportional to our interaction parameter W. Due to enthalpic interactions, the free energy of the brush is now described by:

$$\frac{F}{k_BT} = \frac{L^2}{a^2N_B} + \frac{a^3}{N}(1 - 2N\chi)\frac{N_B^2}{LD^2}. \quad (6)$$

Only positive excluded volumes are allowed such that $(1 - 2N\chi)/N$ should remain positive. From this equation, the transition between mixing and demixing can be obtained:

$$\sigma_{GD,tr} \propto \left(\frac{(1 - 2N\chi)}{N}\right)^{\frac{1}{2}}. \quad (7)$$

Through the phase diagrams for ε_{BB} = 1 with a phase transition present (Fig. 3, top row middle and right), we fitted these theoretical prediction (eqn (5) and (7)) of the mixing to demixing transition. For chemically identical brush and melt (eqn (5)), we introduced a prefactor α, which was utilized as a fitting parameter. This fitting parameter can be related to the effective monomer size and we found it to equal α = 0.82. For the chemically distinct system (W = 0.0625), we introduced a second fitting parameter β to correct for the difference between our interaction parameter $W = \frac{1}{2}(\varepsilon_{BB} + \varepsilon_{LL}) - \varepsilon_{BL}$ and the definition of the Flory Huggins parameter $\chi = \frac{z}{2kT}(\varepsilon_{BB} + \varepsilon_{LL} - 2\varepsilon_{BL})$, resulting in a fit of the form: $\sigma_{GD,tr} = \alpha((1 - 2N\beta\chi)/N)^{\frac{1}{2}}$. From the data obtained for W = 0.0625, we obtained α = 0.82 (kept fixed) and β = 1.75. The fits are shown as black lines in Fig. 3. It is clear that the numerical data are well described by the dependency of eqn (7).

From the geometry-based phase diagrams we see that a shift in W strongly changes the mixing to demixing transition point, as was predicted by eqn (7). This prediction, however, is strictly speaking only valid in the case of positive excluded volume interactions, meaning that $(1 - 2N\chi) > 0$. For our setting of W = 0.0625, this is only the case for N = 8, 4 and 2. Still, for the theoretical prediction at ε_{BB} = 1.0 in Fig. 3, this prediction remains consistent with our numerical results. The data for ε_{BB} = 1.5 cannot be fitted with the same equations, because ε_{BB}, ε_{BL} and ε_{LL} are not equal at W = 0 and, therefore it does not represent chemically identical melts and brushes.

So far, we have discussed the effect of different brush-melt affinities on the transitions in the geometry based phase diagram, as represented in Fig. 3. Now, we would like to discuss how variations in σ_{GD} and N influence the transitions in the interaction-based phase diagram of Fig. 1. In Fig. 1, the black dashed line indicates W_{tr} for mixing to demixing at N = 32 and σ_{GD} = 0.15 chains per σ^2. But, they can be anticipated to change when σ_{GD} and N are varied. Therefore, we determined the transition point in the interaction parameter W_{tr}, for varying values of the polymer melt and the grafting density, and the results are presented in Fig. 4. The datapoints illustrate the shift in the transitions due to entropy for ε_{BB} = 1.0 (blue triangles) and ε_{BB} = 1.5 (green circles) compared to transitions based on enthalpic arguments alone (grey dashed lines).

In Fig. 4(a), W_{tr} is shown as a function of N for σ_{GD} = *0.15 chains per* σ^2. For small chains, the transition occurs at $W > 0$, meaning that entropy is gained by mixing. In contrast, the longer melt chains show a shift to negative W_{tr}, because long chains gain less translational entropy than shorter chains. This smaller amount of entropy gain is not enough to compensate for the entropic penalty to stretch the polymer brush in order to mix. Fig. 4(b) depicts W_{tr} for varying σ_{GD} with N = 32, indicating

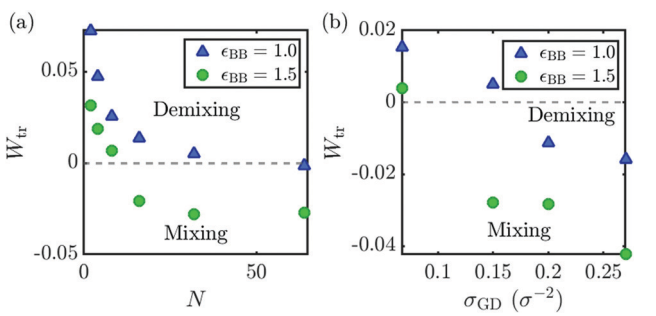

Fig. 4 The interaction parameters W_{tr} at which the mixing to demixing transition occurs, as determined from the overlap integral, (a) for a defined melt length N, and (b) grafting density σ_{GD}. The gray dashed lines in both figures describe the transition using predictions based on enthalpic arguments alone.

a shift to positive W_{tr} for lower grafting density brushes, and a lower, negative W_{tr} for higher grafting densities. This effect of the grafting density is caused by densely grafted brushes having to pay a higher entropic penalty for stretching upon mixing, compared to less densely grafted brushes.

In summary, when regarding only enthalpic interactions, the mixing to demixing transition occurs at $W = 0$. Entropic interactions can increase or decrease W_{tr}, depending on N and σ_{GD}, where shorter chains and lower grafting densities tend to increase W_{tr}, meaning that entropy is gained from mixing. Our simulations for both chemically identical and chemically distinct brushes and melts, show good agreement to theoretical predictions from eqn (7) on the occurrence of the mixing to demixing transition. We have compared this theoretical transition both to a direct geometry-based phase diagram of our system, and to exact predictions of this transition, based on our data.

3.2 Partial wetting–complete wetting

We now focus on the transition from partial wetting to complete wetting. For the demixed states in Fig. 3, we made the distinction between complete wetting (orange triangles) and partial wetting (yellow circles). In the case of $\varepsilon_{BB} = 1.0$ we see a transition directly from mixing to partial wetting for all grafting densities except the highest, where a complete wetting state is observed. For $\varepsilon_{BB} = 1.5$ we observe a transition from mixing to complete wetting. One can expect a complete to partial wetting transition for $\varepsilon_{BB} = 1.5$ too, but for higher values of W only, as is also illustrated in Fig. 1.

Next, we will consider the effect of the grafting density and melt polymer length on the interaction-based phase diagram of Fig. 1. To do so, we plot in Fig. 5 the contact angles (determined by spherical fits to isodensity profiles of the melt droplet[37]) as a function of the interaction parameter W for the different melt-polymer lengths (left graph $\varepsilon_{BB} = 1.5$ and middle graph $\varepsilon_{BB} = 1.0$) and grafting densities (right graph). The data shows an increasing θ for increasing W, caused by the lower brush–melt interactions for higher interaction parameters, that directly influence the wettability between the brush and melt. The data also reveals an increased wettability for shorter melt chains. For example for $W = 0.375$, we observe a contact angle of 78° for larger chains ($N \leq 16$), while it reduces to $\theta < 50°$ for $N = 2$.

chains[57] (see also ESI,† Fig. S3). Moreover, analysis of the density profiles indicate that the overlap integral increases for melts of decreasing chain length, which shows that there is more mixing between the melt and the brush for shorter melt chains. Interestingly, the penetration depths, which we define as the full width half maximum of the peak in $\rho_B\rho_M(z)$, is not affected by the chain length of the melt (*e.g.* at $W = 0.375$ and $\varepsilon_{BB} = 1.5$, the penetration depth is $1.9 \pm 0.3\sigma$) for all N. This means that the system of short chains increases its mixing entropy by decreasing the contact angle and, thus, increasing the contact area.

Our results on the increased wettability for shorter melt chains are in qualitative agreement with experimental contact angle measurements of alkane droplets on poly(dimethylsiloxane),[58] which indeed showed that the contact angle decreases upon decreasing the length of the alkane-chain. The right graph depicts θ plotted against W for varying σ_{GD}. This data illustrates the rather weak dependency of the contact angle on the grafting density, also in agreement with experimental observations.[58]

To examine how the complete to partial wetting transition in the interaction-based phase diagram (Fig. 1) changes upon varying the brush grafting density or melt chain length, we extract W_{tr} from Fig. 5 by interpolating an exponential function fitted to the contact angles in Fig. 5. The W_{tr} between partial and complete wetting is the W for which θ has reached 0. The resulting W_{tr} is shown in Fig. 6, as a function of N (left), and of σ_{GD} (right). The wetting transitions based on the enthalpic estimate $\varepsilon_{LL} = \varepsilon_{BL}$ are given as the blue and green dash-dotted lines, for $\varepsilon_{BB} = 1.0$ and $\varepsilon_{BB} = 1.5$, respectively.

In the left graph of Fig. 6, we see a rise in W_{tr} to positive values for very short chains N. We can explain this through the increased wettability for small N, that was observed from Fig. 5. As mentioned, short chains have lower surface tensions γ_{BL} and

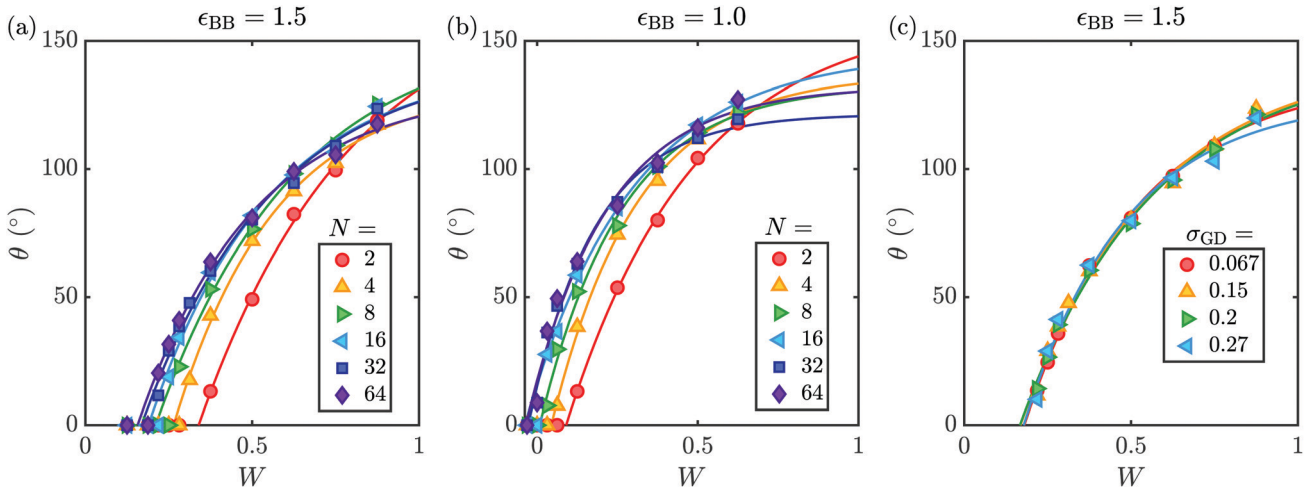

Fig. 5 Contact angles for varying degrees of the interaction parameter W. (a) Shows the contact angles θ for a brush wetted by a melt of varying degrees of polymerization N, at $\varepsilon_{BB} = 1.5$ and $\sigma_{GD} = 0.15$. (b) Shows the contact angles of varying melt chain lengths at $\varepsilon_{BB} = 1.0$ and $\sigma_{GD} = 0.15$. (c) Depicts the influence of the brush grafting density σ_{GD} on the contact angles for $N = 32$.

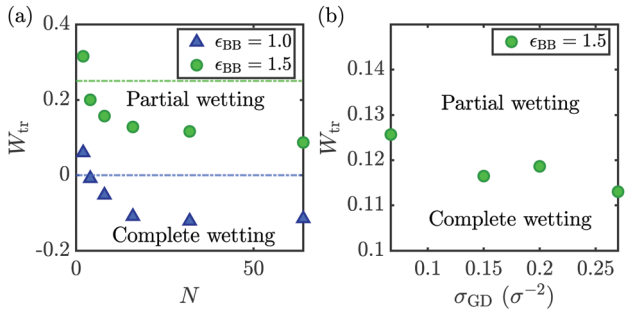

Fig. 6 The interaction parameter transition points W_{tr}, for complete to partial wetting, are plotted as (a) a function of the melt chain length N, and (b) the grafting density σ_{GD}. The wetting transitions based on an enthalpic estimate are given as the blue and green dash-dotted lines, for ε_{BB} = 1.0 and ε_{BB} = 1.5, respectively.

γ_{LV} (see also ESI,† Fig. S3), owing to a higher entropic contribution to the free energy for shorter chains as compared to longer chains. For longer chains, we reach a constant value for W_{tr}, as their surface tensions become similar (see Fig. 5). We assume this is caused by a limit to the intermolecular forces that can significantly contribute to the surface tension of a liquid melt.

The right graph of Fig. 6 shows the dependency of W_{tr} on the grafting density. We observe that W_{tr} slightly decreases upon increasing the grafting density. As mentioned above, the reason for this is the rather weak dependency of the spreading parameter on the grafting density, which is also in agreement with predictions from de Gennes.[59]

The data from Fig. 6(a) can be compared directly to the interaction-based phase diagram of Fig. 1. By doing so, we can compare how wetting transitions shift by changing the polymer melt length. From our data, we find that shorter N values would cause the complete to partial wetting transition to shift to the right, compared to the interaction-based phase diagram of Fig. 1 (here, transitions are marked using black lines), which determined for N = 32. In fact, for the shortest melt chains, our N_{tr} also shifts past the theoretical predictions as given in Fig. 1 (gray lines).

To conclude this section, we demonstrate that a transition from complete to partial wetting strongly depends on the length of the melt polymers N and depends only slightly on the grafting density σ_{GD}. Furthermore, we report greater wettability for shorter melt chains, due to their having a lower surface tension than their longer counterparts.

4 Conclusions

In summary, our results illustrate that wetting transitions are shifted due to entropic effects compared to predictions based on enthalpic effects alone. This shift depends on the length of the melt polymer N and the brush grafting density σ_{GD}. When regarding only enthalpic interactions, the mixing to demixing transition occurs at W_{tr} = 0. Entropic interactions can increase or decrease W_{tr}, depending on N and σ_{GD}, where shorter chains and lower grafting densities tend to increase W_{tr}, meaning that entropy is gained from mixing. The opposite is true for long chains and high grafting densities, where mixing decreases the entropy such that W_{tr} decreases to values below 0. Our results for both chemically identical and chemically distinct brushes and melts show good agreement to mean field theory describing the effect of N and σ_{GD} on the mixing to demixing transition. When considering the transition from complete to partial wetting, we find that short melt chains show higher wettability, meaning that they gain more translational entropy upon wetting a surface completely, as compared to long melt chains. As a result, the interfacial free energies for short chains, γ_{BL} and γ_{LV}, are smaller. Therefore, there is a strong effect of N on W_{tr} and complete wetting is observed for small N even for very high melt–melt interactions. In contrast, we observe that the complete to partial wetting transition depends only weakly on the grafting density. This indicates that, for the partial to complete wetting transitions, the brush can in many situations be regarded as a simple polymer film. Nevertheless, our results show that entropic effects have to be incorporated when considering wetting transitions, which is important in the design of potential applications such as brush-based sensors or self-cleaning surfaces.

Conflicts of interest

There are no conflicts to declare.

Acknowledgements

L. M. and J. H. S. acknowledge financial support from ERC (the European Research Council) Consolidator Grant No. 616918. NWO and SurfSara are acknowledged for HPC resources: this work was carried out on the Dutch national e-infrastructure with the support of SURF Cooperative. (L. M. NWO project number 16265 and S. d. B. reference code #45666).

References

1 S. T. Milner, *Science*, 1991, **251**, 905.
2 O. Azzaroni, *J. Polym. Sci., Part A: Polym. Chem.*, 2012, **50**, 3225.
3 W.-L. Chen, R. Cordero, H. Tran and C. K. Ober, *Macromolecules*, 2017, **50**, 4089–4113.
4 I. Tokareva, S. Minko, J. H. Fendler and E. Hutter, *J. Am. Chem. Soc.*, 2004, **126**, 15950–15951.
5 H. Merlitz, G.-L. He, C.-X. Wu and J.-U. Sommer, *Phys. Rev. Lett.*, 2009, **102**, 115702.
6 L. I. Klushin, A. M. Skvortsov, A. A. Polotsky, S. Qi and F. Schmid, *Phys. Rev. Lett.*, 2014, **113**, 068303.
7 M. Chen, W. H. Briscoe, S. P. Armes and J. Klein, *Science*, 2009, **323**, 1698–1701.
8 J. Yu, N. E. Jackson, X. Xu, Y. Morgenstern, Y. Kaufman, M. Ruths, J. J. de Pablo and M. Tirrell, *Science*, 2018, **360**, 1434–1438.
9 Y. Yu, Y. Yao, S. van Lin and S. de Beer, *Eur. Polym. J.*, 2019, **112**, 222–227.

10 J. D. Willott, T. J. Murdoch, G. B. Webber and E. J. Wanless, *Macromolecules*, 2016, **49**, 2327–2338.
11 Y. Yu, R. A. Lopez de la Cruz, B. D. Kieviet, H. Gojzewski, A. Pons, G. J. Vancso and S. de Beer, *Nanoscale*, 2017, **9**, 1670–1675.
12 H. Yang, H. Zhu, M. M. R. M. Hendrix, N. J. H. G. M. Lousberg, G. de With, A. C. C. Esteves and J. H. Xin, *Adv. Mater.*, 2013, **25**, 1150–1154.
13 J. A. Howarter and J. P. Youngblood, *Adv. Mater.*, 2007, **19**, 3838–3843.
14 A. Halperin and P. G. de Gennes, *J. Phys.*, 1986, **47**, 1243–1247.
15 D. Long, A. Ajdari and L. Leibler, *Langmuir*, 1996, **12**, 1675–1680.
16 C. M. Wijmans, E. B. Zhulina and G. J. Fleer, *Macromolecules*, 1994, **27**, 3238–3248.
17 L. I. S. Mensink, J. H. Snoeijer and S. de Beer, *Macromolecules*, 2019, **52**, 2015–2020.
18 P. G. de Gennes, *Macromolecules*, 1980, **13**, 1069.
19 M. Aubouy and E. Raphael, *J. Phys. II*, 1993, **3**, 443–448.
20 G. S. Grest, *Phys. Rev. Lett.*, 1996, **76**, 4979.
21 P. G. Ferreira, A. Ajdari and L. Leibler, *Macromolecules*, 1998, **31**, 3994–4003.
22 J. H. Maas, G. J. Fleer, F. A. M. Leermakers and M. A. Cohen Stuart, *Langmuir*, 2002, **18**, 8871–8880.
23 C. Pastorino, K. Binder, T. Kreer and M. Müller, *J. Chem. Phys.*, 2006, **124**, 064902.
24 G. Reiter and R. Khanna, *Phys. Rev. Lett.*, 2000, **85**, 5599–5602.
25 X. Zhang, F. K. Lee and O. K. C. Tsui, *Macromolecules*, 2008, **41**, 8148–8151.
26 M. Aubouy, G. H. Fredrickson, P. Pincus and E. Raphael, *Macromolecules*, 1995, **28**, 2979–2981.
27 F. Zhou and W. T. S. Huck, *Phys. Chem. Chem. Phys.*, 2006, **8**, 3815.
28 K. Park, S. H. Park, E. Kim, J.-D. Kim, S.-Y. An, H. S. Lim, H. H. Lee, D. H. Kim, D. Y. Ryu, D. R. Lee and J. H. Cho, *Chem. Mater.*, 2010, **22**, 5377–5382.
29 S. Liu, R. Eijkelenkamp, J. Duvigneau and G. J. Vancso, *ACS Appl. Mater. Interfaces*, 2017, **9**, 37929–37940.
30 G. S. Grest and K. Kremer, *Phys. Rev. A: At., Mol., Opt. Phys.*, 1986, **33**, 3628.
31 S. de Beer and M. H. Müser, *Soft Matter*, 2013, **9**, 7234.
32 S. de Beer, L. I. S. Mensink and B. D. Kieviet, *Macromolecules*, 2016, **49**, 1070–1078.
33 T. Kreer, *Soft Matter*, 2016, **12**, 3479–3501.
34 K. Kremer and G. S. Grest, *J. Chem. Phys.*, 1990, **92**, 5057–5086.
35 W. Humphrey, A. Dalke and K. Schulten, *J. Mol. Graphics*, 1996, **14**, 33.
36 G. S. Grest and M. Murat, *Macromolecules*, 1993, **26**, 3108–3117.
37 J. H. Weijs, A. Marchand, B. Andreotti, D. Lohse and J. H. Snoeijer, *Phys. Fluids*, 2011, **23**, 022001.
38 S. Plimpton, *J. Comput. Phys.*, 1995, **117**, 1.
39 T. Kreer, M. H. Müser, K. Binder and J. Klein, *Langmuir*, 2001, **17**, 7804.
40 C. Gay, *Macromolecules*, 1997, **30**, 5939–5943.
41 A. D. Kazakov, A. A. Polotsky, E. B. Zhulina, T. M. Birshtein, F. A. M. Leermakers and O. V. Borisov, *Macromolecules*, 2020, **53**, 387–397.
42 A. Milchev, D. I. Dimitrov and K. Binder, *Biomicrofluidics*, 2010, **4**, 032202.
43 M. E. R. Shanahan, *J. Phys. D: Appl. Phys.*, 1987, **20**, 945.
44 E. R. Jerison, Y. Xu, L. A. Wilen and E. R. Dufresne, *Phys. Rev. Lett.*, 2011, **106**, 186103.
45 J. H. Weijs, B. Andreotti and J. H. Snoeijer, *Soft Matter*, 2013, **9**, 8494–8503.
46 Z. Cao and A. V. Dobrynin, *Macromolecules*, 2015, **48**, 443–451.
47 R. Dey, M. van Gorcum, F. Mugele and J. H. Snoeijer, *Soft Matter*, 2019, **15**, 6469–6475.
48 F. Léonforte and M. Müller, *J. Chem. Phys.*, 2011, **135**, 214703.
49 J. N. Israelachvili, *Intermolecular and Surface Forces*, Academic Press, Elsevier, USA, 2011.
50 R. Descas, J.-U. Sommer and A. Blumen, *Macromol. Theory Simul.*, 2008, **17**, 429.
51 L. G. MacDowell and M. Müller, *J. Chem. Phys.*, 2006, **124**, 084907.
52 P. de Gennes, *Scaling Concepts in Polymer Physics*, Cornell University Press, 1979.
53 M. Rubinstein and R. Colby, *Polymer Physics*, Oxford University Press, Oxford, 2003.
54 D. Mukherji, C. M. Marques, T. Stuehn and K. Kremer, *Nat. Commun.*, 2017, **8**, 1374.
55 I. Borukhov and L. Leibler, *Macromolecules*, 2002, **35**, 5171–5182.
56 E. Zhulina and O. Borisov, *J. Colloid Interface Sci.*, 1991, **144**, 507–520.
57 D. N. Theodorou, *Macromolecules*, 1989, **22**, 4578–4589.
58 D. F. Cheng, C. Urata, B. Masheder and A. Hozumi, *J. Am. Chem. Soc.*, 2012, **134**, 10191–10199.
59 P. G. de Gennes, *Rev. Mod. Phys.*, 1985, **57**, 827.
60 S. Hartmann and U. Thiele, *Eur. Phys. J. Spec. Top.*, 2020, **229**, 1819–1832.